Coherent control via weak measurements in P 31 single-atom electron and nuclear spin qubits

Muhonen, J. T.; Dehollain, J. P.; Laucht, A.; Simmons, S.; Kalra, R.; Hudson, F. E.; Dzurak, A. S.; Morello, A.; Jamieson, D. N.; McCallum, J. C.

Important note
To cite this publication, please use the final published version (if applicable).
Please check the document version above.

Brightness measurements of the nano-aperture ion source

Leon van Kouwen, and Pieter Kruit

Articles you may be interested in

Brightness measurements of the nano-aperture ion source

Leon van Kouwen[a)] and Pieter Kruit
Faculty of Applied Sciences, Delft University of Technology, Lorentzweg 1, 2628 CJ Delft, The Netherlands

A new type of ion source capable of delivering bright and monochromatic beams of various ionic species has been developed. The brightness of this source was measured using an ion focusing column in combination with a knife-edge ion transmission detector. The emission current was varied in the range 200 pA to 20 nA by varying the particle density and the in-chip electric field. Most data were obtained using argon ions, but helium and xenon ions were also produced. The setup was used to experimentally demonstrate a brightness of $B \approx 1 10^5$ A/m² sr V. The measurements match reasonably well with ray-trace simulations. *Published by the AVS.*
https://doi.org/10.1116/1.5048054

I. INTRODUCTION

Focused ion beam systems are crucial in today's nanofabrication efforts. The fabrication of TEM lamella or novel nanodevices are examples of popular applications. For many years, the gallium liquid metal ion source has been the industrial standard. It is bright, reliable, cheap, and provides a relatively high current, a sensible all-round choice.

Sometimes, the use of a gallium is undesirable though. For example, when repairing UV nanoimprint masks, the gallium contamination can decrease the transparency of the mask down to unacceptable levels.[1] For mesoscopic thin-films, even the slightest gallium dose can destroy the functionality.[2]

To enable different ionic species, while at the same time deliver comparable or even better performance, many ideas for new ion sources have been introduced. For example, the gas field ionization source (GFIS)[3] enabled quite a few applications.[4] The GFIS technology is not easily extended to heavier gases than neon though.[5] Furthermore, this technology typically only delivers bright beams up to 10 pA. Recent work did demonstrate a bright xenon beam, but the beam current is only about 1 pA.[24]

A different approach is the development of a bright inductively coupled plasma source in order to enable reasonably high resolution while maintaining the merit of high current.[6,25] The achieved brightness of about 1×10^4 A/m² sr V is quite low though for high resolution applications.

Making bright, monoenergetic ion beams using laser cooling was proposed by Freinkman *et al.*[7] The ultracold ion source[8] and the magneto-optical trap ion source[9,10] are examples of this idea. Simulations[11–13] and some experimental work[14,15] of an improved version of this source, using an atomic beam rather than relying on diffusion, look promising.

A source offering a brightness of, say, 1×10^6 A/m² sr V, an energy spread of 1 eV or smaller, and at least 1 nA of current, while offering a variety of desirable species, is likely to become very popular. Therefore, we are committed to develop such an ion source.

We propose an ion source based on electron impact gas ionization inside a submicron sized gas chamber.[16–19] The gas chamber consists of two very thin membranes of about 100 nm thick, which are separated by a small distance of 100 nm to 1 μm, as shown in Fig. 1. A small aperture of 100–500 nm in the membranes allows the ions to escape and a focused electron beam to enter the ionization region while maintaining a high pressure inside the structure. An electric field between the membranes directs the ions toward the exit aperture and ensures fast emission. Outside the membrane structure, an electric field further accelerates the beam up to the desired high energy. This configuration can offer excellent optical performance when using a high current density electron beam and a highly confined ionization region. One embodiment of this technology for generating highly energetic proton beams is also under development.[20,21]

Recent simulations[19] point out that a brightness of over 1×10^6 A/m² sr V is achievable in high-end systems. This is a very promising result, as such brightness is comparable or better than what a typical gallium liquid metal ion source delivers. While the present generation of experimental setup is not sufficient to deliver 1×10^6 A/m² sr V, we aim to demonstrate a competitive value already. Moreover, we compare the theoretical simulations to the experimental results.

II. EXPERIMENTAL METHOD

The goal of this research is to determine the 50% beam brightness B_{50}, defined by

$$B_{50} = \frac{4I_{50}}{\pi^2 d_{50}^2 \alpha_{50}^2 \Phi}. \tag{1}$$

We use d_{50} for the full width 50 (fw50), which defines the region in the focused spot containing 50% of the current. α_{50} is the half-angle of the cone containing 50% of the beam current, I_{50} is the current within that beam cone, and Φ is the electrostatic beam energy.

When brightness is measured, often a beam limiting aperture is used to select a small fraction of the beam. This results in a top-hat angular current distribution, making the beam divergence clearly defined by the steep decrease of this

---

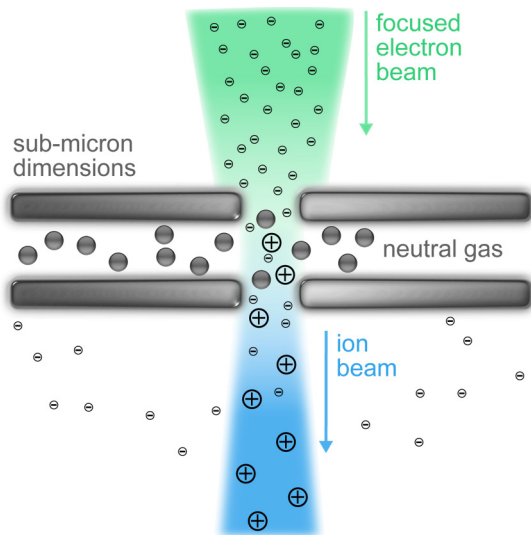a)Author to whom correspondence should be addressed: lvankouwen@gmail.com

FIG. 1. Nano-aperture ion source forming high brightness beams of various species by ionizing a gas confined in a submicron volume using electron beam impact ionization. An electric field between the membranes extracts the ions out of the double-membrane structure.
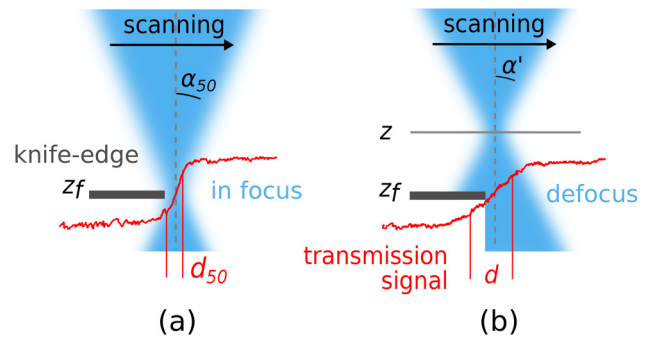

FIG. 2. Knife-edge scanning the ion beam to determine the beam properties. $z = 0$ is located outside of this image at the ion source. (a) The beam is focused on the knife-edge such that the source can be imaged. (b) From defocused scans, the beam divergence angle can be determined.

distribution. In our setup, however, we avoid such a beam limiting aperture to simplify the alignment. The definition in Eq. (1) is more general and unambiguous for any kind of angular distribution and can therefore be used in our no-aperture configuration.

The goal of the experiment boils down to determine the constituents of Eq. (1). The acceleration voltage Φ is something we can simply control. For measuring the total current I_{100}, we let the beam land on a conductor that is biased to +50 V with respect to the surroundings in order to prevent secondary electrons to escape. Obviously, $I_{50} = \frac{1}{2}I_{100}$. For determining the geometrical spot size d_{50}, we need an optical column to form an image of the source. The image formation should not be deteriorated by aberrations, coulomb interactions, or other disturbances that are not related to the source. We use an ion transmission imaging system such that we can make knife-edge scans and infer the spot size from those scans. We use a 25–75% rise distance, assume a Gaussian beam-profile, and convert it as $d_{50} = 1.75 \cdot d_{25-75}$. The beam may deviate from a Gaussian shape, but Bronsgeest et al. showed that this is a good approximation for different distributions as well.[22] By defocusing the beam and making knife-edge scans, we can find the beam divergence angle α_{50}. Figure 2 shows the concept of focused and defocused knife-edge scans.

The method of measuring the brightness of a particular source operation configuration requires a set of different focused and defocused knife-edge scans. We fit the measured probe sizes to a defocus model. The probe size d as a function of the focus position z according to the proposed model is

$$d(z) = \left(d_{50}^s + \left| 2\alpha_{50}(z - z_f) \frac{M_a(z)}{M_a(z_f)} \right|^s \right)^{1/s}. \qquad (2)$$

If the beam is focused on the knife-edge, the smallest probe size is acquired, denoted by d_{50}. The constant z_f is the z-position of the best focused image, i.e., the knife-edge location. M_a is the angular magnification, which depends on the focus position. We defocus the beam by changing the lens voltage. When doing this, we change the beam divergence itself, which we have to correct by including the ratio of angular magnifications in the model. The free parameter s dictates how the defocusing blur and the geometrical spot size are added. Most correct would be a convolution of the distributions, but a power law is often a good approximation. We do not know what power is most appropriate, so we keep it as a free parameter.

The focus position z and the angular magnification M_a cannot be measured directly. We use a ray-tracing simulation to relate the applied lens voltage to these quantities. The set of measured d's with accompanying z-positions and M_a's as acquired from ray-tracing are the input for a least squares fit of Eq. (2). The outputs of the fitting procedure are α_{50} and s, of which the former is the quantity of interest.

In conventional secondary electron detection schemes, rounded edges introduce a blur in the image, which is a known pitfall in probe size measurements.[23] However, we repel any secondary electrons and only transmitted ions are measured. Only ions that penetrate the material and come out again below or on the side can give an error in the measurement. The typical size associated with such a process is in the order of nanometers, which is much smaller than the typical probe size we intend to measure, ranging from 200 nm to 5 μm.

III. EXPERIMENTAL SETUP

We have designed a simple ion optical column that can form an image of the source at the knife-edge location. Figure 3 depicts the general idea of this experimental setup. Note that this setup is designed for measuring source properties but does not offer high resolution capabilities. We use a conventional scanning electron microscope (SEM) to supply the electron beam (FEI Verios). Our device was retrofitted to a so-called SECOM platform supplied by DELMIC. This platform replaces the SEM door and contains several piezo-electric precision stages. The ion optical column can be

moved to make the nano-aperture coincide with the electron optical axis. The detector can be moved to position the knife-edge on the ion optical axis.

The knife-edge sample we use is a pattern of holes of $45.7 \pm 0.2 \, \mu m$ in diameter. This diameter is much larger than the typical probe size we intend to measure such that we may approximate the curved edges as straight. The sample thickness is $54.5 \pm 1 \, \mu m$; thin enough to prevent any significant beam broadening.

The fraction of ions that is transmitted around the knife-edge is being guided to the side by means of an eccentric cavity below the knife-edge. Any secondary electrons originating from the knife-edge are prevented from escaping due to a +50 V bias on the knife-edge. The transmitted ions hit a metal surface and generate secondary electrons. These are in turn accelerated toward the detector at ground potential and end up with 8 keV of kinetic energy. The secondary electron signal is detected by a semiconducting electron detector (Opto Diode AXUV63HS1).

The system is source magnifying, yielding a couple of advantages. A rather large working distance becomes acceptable such that postlens scanning is possible. This makes pivot-point scanning unnecessary, and one octopole for scanning and stigmation is sufficient. Furthermore, any absolute errors, such as mechanical vibrations, become less relevant.

For a good measurement of the source properties, we need to confirm that the aberrations are sufficiently low, as the probe size should be dominated by the source image. We also need to know the relation between the lens voltage and the image z-position in order to compute the beam divergence angle, as explained in the Experimental method section. Therefore, we performed electrostatic field solving and ray-tracing, using the electron optical design (EOD) software.

The results of ray-tracing through the optical system are shown in Table I. A typical normalized beam angle after uniform acceleration for the nano-aperture ion source (NAIS) is $0.15 \, \text{mrad} \, V^{1/2}$.[19] For this setup, considering a 5 kV energy and a magnification of 3.3, the expected beam angle at the knife-edge is 0.7 mrad. This value may range between 0.4 and 1.0 mrad for alternative operation conditions. We use these values to estimate the aberration contributions. We expect a virtual source size between 100 and 300 nm, which at the knife-edge location translates to roughly 300–1000 nm. Since we also make defocused images, the largest measured knife-edge scan sizes may reach several micrometers.

In order to verify that the chromatic aberration is not significantly broadening the probe size, we need to have a rough estimate for the upper bound of the energy spread. Simulations and experiments showed that the energy spread is mostly determined by the bias voltage applied to the membranes.[18] In more detailed simulations, it was shown that the energy spread can be reduced due to gas scattering and increased due to the Boersch effect.[19] The latter only becomes important at a higher brightnesses than those expected in this experiment. For rough estimates, a reasonable rule-of-thumb is that the energy spread in terms of fw50 is roughly equal to half the applied bias voltage. Our upper bound estimates for 0.6, 4.3, and 10.3 V bias are, respectively, 1, 4, and 10 eV. Note that for the lowest bias voltage, the nominal case, we are a little bit more conservative because field penetration of the extraction field gives a small contribution to the energy spread.

Comparing the typical expected probe sizes to the results shown in Table I, we can expect the virtual source image to be the dominant probe contributor in most cases. Spherical aberration plays no role in the probe formation at all. This means that nonchromatic off-axis aberrations should be relatively small as well, as they are linked to the spherical aberration coefficient. In high current operation, when the energy
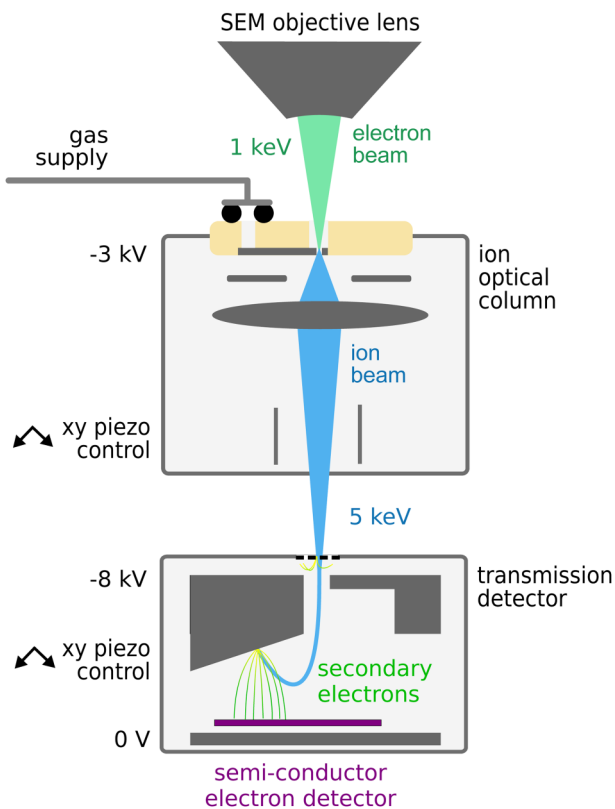

FIG. 3. Experimental setup is an ion optical column inside a scanning electron microscope. Additionally, we use a Delmic SECOM platform for the xy control of the ion optical column and independently the ion transmission detector together with the knife-edge sample.

TABLE I. Ion optical simulation is performed using the EOD software, from which we have calculated optical properties under nominal operation of the setup. This simulation considers a virtual source that already includes any optical effects caused in and around the chip. An energy spread of 1 eV is assumed.

Magnification	M	3.3	
Chromatic aberration coefficient	C_c	1.0×10^3	mm
Spherical aberration coefficient	C_s	3.6×10^4	mm
Beam divergence angle	α_{50}	0.7	mrad
Source image probe contribution	d_g	300–1000	nm
Spherical aberration probe contribution	d_s	2.2	nm
Chromatic aberration probe contribution	d_c	84	nm
Acceleration voltage	Φ	5	kV
Extraction field	E_{acc}	3.3	kV/mm

spread is several eV and the beam divergence is relatively large, the chromatic aberration can become comparable to the geometrical contribution.

Some limitations to the system prevent us from reaching a brightness above 1×10^6 A/m^2 sr V. When operating the FEI Verios SEM at 121 nA and 1 keV landing energy, we estimate an electron beam fw50 probe size of 230 nm. In comparison, a system with a better optimization in the high current regime could produce 100 nA in a 50 nm fw50.[18] Furthermore, the ion optical system uses a 3.3 kV/mm acceleration voltage right after ion emission, while 10 kV/mm is desirable. Nevertheless, our simulations[19] indicate that $B \approx 1 \times 10^5$ A/m^2 sr V is possible with the presented experimental setup.

The nanofluidic device has an estimated membrane spacing of 1200 nm with a 675 nm aperture diameter on the electron side and a 800 nm diameter aperture on the ion side. We align the device with respect to the ion optical column by letting the KOH etch sides touch three precision spheres. In principle, this method can offer 5 μm alignment accuracy, but in practice, we achieved an estimated 27 μm alignment accuracy.

IV. RESULTS

Figure 4(a) shows an example ion transmission image using argon ions. For the final beam property analysis, we use horizontal line scans. The acquired line scans were most often comparable to the one in Fig. 4(b). From such a line scan, an unambiguous rise distance is easily determined. Figure 4(c) shows one example of a line scan that can lead to an erroneous rise distance. Such line scans are rejected based on visual inspection. We attribute the differences to a combination of beam a-symmetry and detector response non-uniformity. For any particular detector aperture and operation condition of the source, the line scan shape was stable, so we do not attribute the issue to source instability. Since the non-transmitting part of the line scan (left-hand side of the curves in Fig. 4) suffered less from such nuisances, we found it is more robust to use only the left-hand side of the steepest part in the line scan to determine the rise distance. Effectively, we have defined the 25–75% rise distance as twice the 25–50% distance.

The large set of line scans for various operating conditions are fitted according to the model of Eq. (2). An example fit is shown in Fig. 4(d). The quality of fitting the model varies between operating conditions. In particular, we find that measurements with a positive defocus ($z > z_f$) do not always match the model very well. We have found no satisfying explanation for this inaccuracy. The result of inaccurate fits is a relatively large uncertainty in determining the beam divergence angle.

The results of the model fits are used to compute brightnesses according to Eq. (1). The results are shown in Fig. 5. The perhaps obvious but most important observation is the experimental demonstration of $B \approx 1 \times 10^5$ A/m^2 sr V. A very promising result as well is a brightness of 3.5×10^4 A/m^2 sr V at 20 nA of emission current. This shows that also in the relatively high current regime, the NAIS is a viable concept.
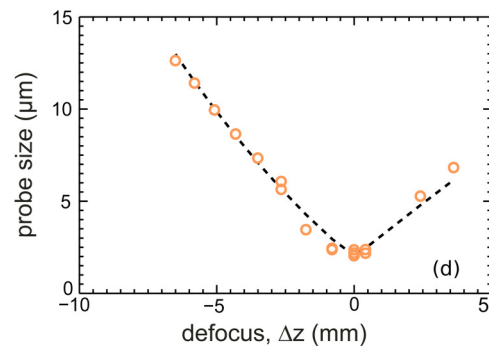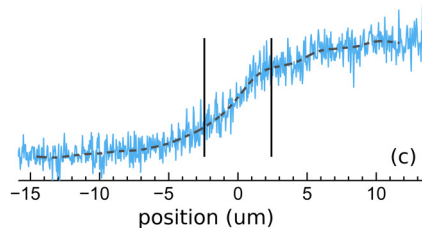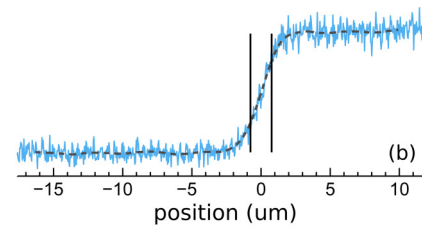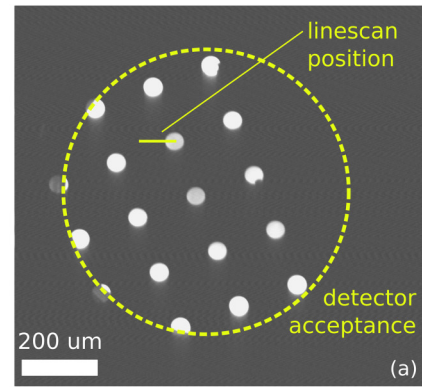

FIG. 4. (a) Ion transmission image of the full sample. (b) A high quality line scan. (c) A refuted line scan. (d) Example of a defocus measurement with a fit of the model given by Eq. (2); 5.0 nA beam current, 0.6 V bias.

During the experiments, we have varied the inlet pressure to obtain different emission currents. We plot the brightness as a function of the emission current rather than the inlet pressure such that the graph indicates the performance more clearly. This also enables comparison to simulations, shown in the same figure. The experimental data follow the trend of the simulations roughly. For low currents, the brightness increases with increasing current, while later the brightness saturates. This corresponds to balancing the added current with increased gas scattering and coulomb interactions.
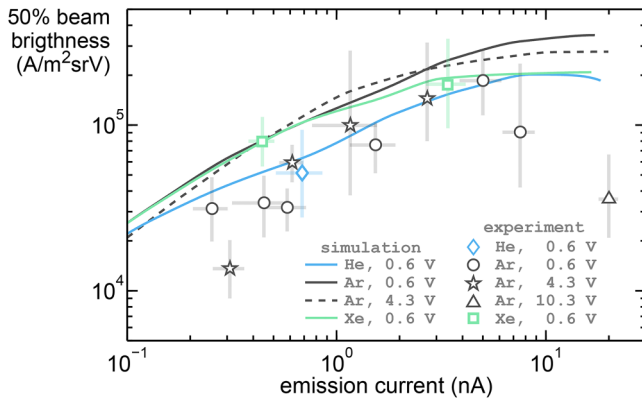
FIG. 5. Measured brightness. For a particular gas species and membrane bias voltage, we obtain different emission currents by varying the gas inlet pressure. The error bars in the current represent minimum and maximum values measured. The error bars in the brightness are a combination of the 95% confidence interval of the model fitting and the error in the emission current. The simulated curves are based on the model discussed elsewhere (Ref. 19), using the dimensions and electron beam settings as acquired during the experiments. Only the acceleration region is included in the simulations. The indicated voltages refer to the applied membrane bias voltage.

The data and simulations are comparable in order of magnitude, but the measured data for argon are systematically less bright. Xenon and helium data match the simulation rather well; however, this should be considered coincidental due to the limited amount of data points and the relatively large uncertainties. The highest current data point (triangle) in particular shows a considerable lower brightness than the simulations predict. At such a high current, it is likely that trajectory displacement due to coulomb interactions in the decelerating lens deteriorates the beam. Furthermore, the bias voltage was set to 10.3 V and we estimate an energy spread of up to 10 eV in that case. The chromatic aberration is proportional to the energy spread, so based on Table I, we can expect a 800 nm chromatic aberration probe contribution. Note that both these probe broadening effects are artifacts of the measurement system and not limitations to the brightness of the source.

The measured current includes a rather large spread (10–50%). We found a lower current when the ion beam was focused on the detection plate than when defocused. The detection plate was biased to +50 V, so we believe that almost no secondary electrons's can escape. Potential influences can be back-scattered ions, secondary ions, and local charging; however, no satisfying complete and consistent explanation was found. The minimum and maximum measured values are introduced as error bars in Fig. 5. These minimum and maximum values are also added to the brightness uncertainty stemming from beam angle uncertainty. The uncertainty in the brightness is no longer strictly defined as a 95% confidence interval but can be interpreted as a 95% or better chance of finding the real brightness within the error bars, under the assumption that no other errors are significant.

We can inspect the virtual source size and the beam angle in Fig. 6 to understand the obtained brightness measurements better. The virtual beam angle is weakly increasing with inlet pressure, as expected from simulations. Also, the beam angle values are in the right ballpark when comparing to the simulations.
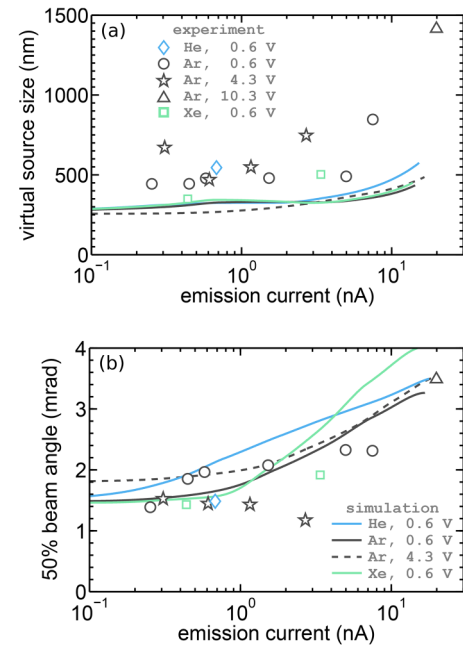

FIG. 6. Source size and source angle in the virtual source plane are the constituents of the brightness measurements shown in Fig. 5. The virtual source is defined after acceleration up to 5 keV but excludes the lens effect of the extractor electrode. The simulated curves are based on the model discussed elsewhere (Ref. 19), using the dimensions and electron beam settings as acquired during the experiments. Only the acceleration region is included in the simulations. The indicated voltages refer to the applied membrane bias voltage.

The virtual source size is more puzzling. At least in the lower current regime we expect the virtual source size to reflect the electron beam size, so a 200–300 nm fw50. We see this in the simulations but not in the measured data. The measured data are more or less a factor 2 larger than expected and show unexpected variation between the data points.

It seems a resolution limit in our measurement system is the current bottleneck, rather than the source itself. We have tried to confirm this by generating a smaller virtual source size. When using 3 kV and 13.3 nA, the electron beam probe size was 33 nm spot size. The measured virtual source size was 684 nm, which is comparable to the measurements with the bigger electron beam. In contrast, when deliberately enlarging the virtual source size, the measured virtual probe size does increase. Apparently, the probe size measurements do not purely yield the virtual source size but represent a lower bound. We have not been able to identify the cause of the error. Because there is no clear trend visible when considering the different gas species, the probe size growth is unlikely to be caused by coulomb interactions.

V. CONCLUSIONS

An argon ion beam brightness of $B \approx 1 \times 10^5$ A/m^2 sr V is demonstrated experimentally. The experimental results were in reasonable agreement with the simulation model, although the measured brightness was somewhat lower than predicted. From our experimental results, we conclude that the brightness is limited mainly by a too large virtual source size.

We estimate that the brightness could potentially be at least one order of magnitude higher. We identify inadequate electron beam performance, too weak ion acceleration field, and too low ion lens voltage as known issues preventing $B \geq 1 \times 10^6$ A/m^2 sr V. Furthermore, the experimental setup comprises an unknown source of resolution deterioration that needs to be addressed.

Although there is clearly room for improvement, the experimental results achieved already demonstrate that the nano-aperture ion source is a viable concept for high resolution ion beam applications.

ACKNOWLEDGMENTS

[1]S. Waid, H. D. Wanzenboeck, M. Gavagnin, R. Langegger, M. Muehlberger, and E. Bertagnolli, J. Vac. Sci. Technol. B **31**, 041602 (2013).

[2]J. Barzola-Quiquia, S. Dusari, G. Bridoux, F. Bern, A. Molle, and P. Esquinazi, Nanotechnology **21**, 145306 (2010).

[3]B. W. Ward, J. Vac. Sci. Technol. B **24**, 2871 (2006).

[4]G. Hlawacek, V. Veligura, R. van Gastel, and B. Poelsema, J. Vac. Sci. Technol. B **32**, 020801 (2014).

[5]F. H. M. Rahman, S. McVey, L. Farkas, J. A. Notte, S. Tan, and R. H. Livengood, Scanning **34**, 129 (2012).

[6]N. S. Smith, W. P. Skoczylas, S. M. Kellogg, D. E. Kinion, P. P. Tesch, O. Sutherland, A. Aanesland, and R. W. Boswell, J. Vac. Sci. Technol. B **24**, 2902 (2006).

[7]B. G. Freinkman, A. V. Eletskii, and S. I. Zaitsev, Microelectron. Eng. **73–74**, 139 (2004).

[8]S. B. van der Geer, M. P. Reijnders, M. J. de Loos, E. J. D. Vredenbregt, P. H. A. Mutsaers, and O. J. Luiten, J. Appl. Phys. **102**, 094312 (2007).

[9]J. L. Hanssen, J. J. McClelland, E. A. Dakin, and M. Jacka, Phys. Rev. A **74**, 063416 (2006).

[10]B. Knuffman, A. V. Steele, J. Orloff, and J. J. McClelland, New J. Phys. **13**, 103035 (2011).

[11]S. H. W. Wouters, G. ten Haaf, R. P. M. J. W. Notermans, N. Debernardi, P. H. A. Mutsaers, O. J. Luiten, and E. J. D. Vredenbregt, Phys. Rev. A **90**, 063817 (2014).

[12]G. ten Haaf, S. H. W. Wouters, S. B. van der Geer, E. J. D. Vredenbregt, and P. H. A. Mutsaers, J. Appl. Phys. **116**, 244301 (2014).

[13]B. Knuffman, A. V. Steele, and J. J. McClelland, J. Appl. Phys. **114**, 044303 (2013).

[14]G. ten Haaf, S. H. W. Wouters, P. H. A. Mutsaers, and E. J. D. Vredenbregt, Phys. Rev. A **96**, 053412 (2017).

[15]A. V. Steele, A. Schwarzkopf, J. J. McClelland, and B. Knuffman, Nano Futures **1**, 015005 (2017).

[16]D. S. Jun, V. G. Kutchoukov, and P. Kruit, J. Vac. Sci. Technol. B **29**, 06F603 (2011).

[17]V. N. Tondare, "Towards a high brightness, monochromatic electron impact gas ion source," Ph.D. thesis (Delft University of Technology, 2006), see https://repository.tudelft.nl.

[18]D. S. Jun, "Development of the nano-aperture ion source (NAIS)," Ph.D. thesis (Delft University of Technology, 2014), see https://repository.tudelft.nl.

[19]L. van Kouwen, "The nano-aperture ion source," Ph.D. thesis (Delft University of Technology, 2017), see https://repository.tudelft.nl.

[20]N. Liu, X. Xu, R. Pang, P. Santhana Raman, A. Khursheed, and J. A. van Kan, Rev. Sci. Instrum. **87**, 02A903 (2016).

[21]X. Xu, P. Santhana Raman, R. Pang, N. Liu, A. Khursheed, and J. A. van Kan, Nucl. Instrum. Methods Phys. Res. A **404**, 52 (2017).

[22]M. S. Bronsgeest, J. E. Barth, L. W. Swanson, and P. Kruit, J. Vac. Sci. Technol. B **26**, 949 (2008).

[23]J. Orloff, Proc. SPIE **7729**, 77290C (2010).

[24]W.-C. Lai, C.-Y. Lin, W.-T. Chang, P.-C. Li, T.-Y. Fu, C.-S. Chang, T. T. Tsong, and I.-S. Hwang, Nanotechnology **28**, 255301 (2017).

[25]S. Kellogg, R. Schampers, S. Zhang, A. Graupera, T. Miller, W. Laur, and A. Dirriwachter, Microsc. Microanal. **16**, 222 (2010).